

Article

Implementation of High Gas Barrier Laminated Films Based on Cellulose Nanocrystals for Food Flexible Packaging

Ghislain Fotie ^{1,*}, Stefano Gazzotti ^{2,3}, Marco Aldo Orteni ^{2,3} and Luciano Piergiovanni ¹

¹ DeFENS, Department of Food, Environmental and Nutritional Sciences, Università degli Studi di Milano, Via Celoria 2, 20133 Milano, Italy; Luciano.Piergiovanni@unimi.it

² Dipartimento di Chimica, Università degli Studi di Milano, Via Golgi 19, 20133 Milano, Italy; Stefano.Gazzotti@unimi.it (S.G.); Marco.Orteni@unimi.it (M.A.O.)

³ CRC Materiali Polimerici “LaMPo”, Dipartimento di Chimica, Università degli Studi di Milano, Via Golgi 19, 20133 Milano, Italy

* Correspondence: Ghislain.Fotie@unimi.it

Received: 7 April 2020; Accepted: 30 April 2020; Published: 4 May 2020



Abstract: In this work, three types of cellulose nanocrystals (CNCs) were used: CNC_{SO₃H} extracted from wood pulp by sulfuric acid (H₂SO₄), CNC_{COOH} extracted from cotton linters by ammonium persulfate (APS) and CNC_{COOR} obtained by esterification of the previous two CNC_{COOH} and CNC_{SO₃H}. For a comparative assessment of gas barrier performance, plastic films such as PLA, PET, PE, PP, OPP and OPA were selected, coated with the three types of CNCs and finally laminated with a solvent-based polyurethane adhesive. First, all dispersed CNCs were characterized by apparent hydrodynamic diameter and Z potential by means of dynamic light scattering (DLS) and electrophoretic light scattering (ELS) techniques, respectively, followed by the crystallinity index (XRD), thermogravimetric analysis (TGA) and evaluation of Fourier-transform infrared spectroscopy (FTIR), as well as the charges density. The surface chemistry of coated plastics (CNCs-P) was assessed by the Z potential through the electrokinetic technique (streaming potential method) and the optical contact angle (OCA). Lastly, laminated films (P-CNC-P) were evaluated by gas permeability measurements at 23 °C and 50–80% RH. It is worth noting that improvements between 90% and 100% of oxygen barrier were achieved after the lamination. This paper provides insights on the choice of cellulosic nanomaterials for the design and development of advanced and sustainable food packaging materials.

Keywords: Cellulose nanocrystals modification; Cellulose nanocrystals coatings; lamination; Food packaging applications

1. Introduction

Cellulose nanocrystals (CNCs) surface chemistry and shape may be utterly different, depending on the type of the extraction and the raw materials used. Generally, CNCs extraction consists of an acidic or oxidative hydrolysis of cellulosic sources (cotton linters, vegetal by-products, wood pulp, etc.). As reported in many papers, CNCs extracted by hydrochloric acid (HCl) are uncharged [1], while those obtained by sulfuric acid (H₂SO₄) contain sulfate half ester charges [2–4], and those extracted by 2,2,6,6-Tetramethylpiperidin-1-yloxy (TEMPO) and ammonium persulfate (APS) contain carboxylic charges on their surface [5,6]. It bears mentioning that the superficial chemical charges dictate the dispersibility of the CNCs in solvent or water [7,8] and the strength of adhesion during the interaction CNCs/polymer [9]. Due to their many positive features, like tiny size and high crystallinity, CNCs may be implemented in food packaging materials, in particular as coatings on plastic films, with a consequent

enhancement of gas barrier properties [10–12]. In addition, it has been shown that in dry conditions, with a thickness of about 1 μm , CNCs coatings displayed an oxygen barrier higher than that obtained from 3 μm to 4 μm thickness of common synthetic barriers, such as Ethylene vinyl alcohol copolymer (EVOH) and Polyvinylidene chloride homopolymer (PVDC), currently used for the extension of oxidation sensitive foods [13]. However, it has also been revealed that the interaction polymer/CNCs is not the same for all polymers, and therefore investigation must be conducted to establish a broad knowledge on the polymers and CNCs chemistry for being ascertained by their chemical affinity and adhesion throughout the coating process. Recent studies have demonstrated that the relevance of the CNCs barrier against gases are lost in humid atmospheres, with a subsequent increase in permeation of gases [14–16]. From the reported findings, CNCs, being very hydrophilic and hygroscopic materials, tend to integrate water, followed by a gradual disentanglement of their crystalline lattice, which then facilitates the gases to cross the coated plastic films even abruptly [16]. Several attempts have been made in order to alleviate that inconvenience by producing more hydrophobic CNCs through their surface chemical modifications, such as esterification, carbamation, silylation, amidation and surfactant adsorption [17–20]. It is likely that esterification represents one of the most versatile and widespread functionalization pathways of cellulose nanocrystals. Most esterification reactions, such as solvent-free esterification [21,22], Fischer esterification [23] and transesterification usually use a chemical compound for grafting [24], which most often severely impacts the morphology and the crystallinity of the modified CNCs [25]. For keeping unblemished the crystallinity of the esterified CNCs and lowering the degree of substitution, in this paper, in situ esterification was promoted between crystals (CNCs-CNCs) without a grafting agent, using APS not only as an oxidizing agent, but also as a catalyst for the esterification. It is important to underline that, for reasons of convenience; CNCs from two different sources have been used to perform the esterification: $\text{CNC}_{\text{SO}_3\text{H}}$ from wood pulp were purchased, while CNC_{COOH} from cotton linters were produced in our laboratory. Even though some researchers successfully implemented hydrophobic CNCs, the gas barrier properties of the coated polymers with those modified crystals were lost or slightly improved, but not at acceptable and relevant standards for being applied in packaging [26–28]. In food packaging, the lamination technique has long been used to combine various materials with different properties in order to obtain complex multi-layers' structures, which complied with all the requirements in terms of gas barrier (O_2 and CO_2), grease resistance, water barrier and sealable-mechanical properties. As mentioned above, one of the common synthetic laminated resins currently used for shelf-life extension is the EVOH, whose structure of which is also strongly sensitive to water, and behavior of which is similar to CNCs in a wet environment [29]. For overcoming that drawback, the lamination technique has been adopted to protect the EVOH layers from the surrounding environment, and that contributed to make possible their use in modern food packaging applications [30]. In this paper, in situ esterification was successfully achieved by introducing ester groups on CNCs and, subsequently, laminated multi-layers based on the coatings of modified and neat CNCs were successfully set up by the confinement of the CNCs layer between water-repellent materials. This work revealed that the esterification did not affect the CNCs crystallinity, and that the lamination proved very effective in mitigating the water sensitivity of CNCs coatings, thereby significantly improving the oxygen barrier properties.

2. Materials and Methods

2.1. Materials

Plastic films, such as 12 μm -thick PET (polyethylene-terephthalate), 75 μm -thick PE (polyethylene), 40 μm -thick PP (polypropylene), 15 μm -thick OPA (oriented polyamide), 30 μm -thick OPP (oriented polypropylene), 25 μm -thick PLA and POLURFLEX 2644/58-01, a two-component polyurethane solvent based adhesive system [mixing ratio 100:10:83 (OH: NCO: Solvent)] with 13 s viscosity 25 $^\circ\text{C}$ were all provided by Sapici spa, Cernusco sul Naviglio, Italy. Cellulose nanocrystals obtained by acid hydrolysis ($\text{CNC}_{\text{SO}_3\text{H}}$) of the wood pulp were bought from CelluForce 609, Rang 12C.P.1010 Windsor (Quebec).

2.2. Methods

2.2.1. Carboxylated and Esterified Cellulose Nanocrystals Preparation

Carboxylated CNCs were produced by APS (ammonium persulfate) hydrolysis scrupulously following the route proposed by Leung and co-workers [5]. Esters groups were obtained when carboxylic and hydroxyl compounds reacted in an acid media. For esterified CNCs production, 10 g of grinded cotton linters were mixed with 20 g of cellulose nanocrystals obtained by sulfuric acid (CNC_{SO₃H}) in distilled water, containing 1M APS (m/V) at 75 °C for 16 h. At the end of the reaction, the color of the solution shifted from white to yellow. The latter solution was then cooled, centrifuged (9000 rpm × 15 min × 3 times), brought to pH 7 and finally sonicated for 10 min at 180 W power and 80% amplitude, followed by three-stage filtration. In addition to the confirmation of the presence of ester groups by Fourier-transform infrared spectroscopy (FTIR) analysis, the color shift from white to yellow was also considered an indicator of the esterification occurrence.

2.2.2. Charges Density Assessment

Both Z potential and conductometric titration were used to monitor charges density and colloidal stability of water-suspended cellulose nanocrystals. Zeta potential (mV) and conductivity (mS cm⁻¹) of the CNCs in the diluted water-suspension CNCs 0.5 wt% at pH 6 were determined by electrophoretic light scattering (ELS), using the PALS technology (mod. Litesizer 500, Anton Paar, Graz, Austria). Measures were replicated 5 times, at 25.0 ± 0.1 °C, by means of a 35-mW diode laser (λ = 658 nm) and at a 15° detection angle. Conductometric titration was used to evaluate weak and strong acids in the three suspended samples: CNC_{COOH}, CNC_{COOR} and CNC_{SO₃H}. A total of 15 mg of CNCs were suspended in 200 mL of distilled water and sonicated for 5 min. The pH of the suspension was then brought to 3 with HCl 0.1 M before the titration. The apparatus is constituted of a pHmeter and conductivity meter (Multi3620 IDS) and a titrator (Si Analytics Model Titronic 300, YSI, 1725 Brannum Lane, Yellow Springs, OH, USA). NaOH 0.01 M was dispensed in diluted CNCs at 100 ml increments, and stirred for 1 min, before collecting the electric conductivity (μS/cm). While the sodium hydroxide (NaOH) is added through the titration, the conductivity first decreases to reach a constant and stable plateau briefly and after, it increases to reach a constant value of electric conductivity. The charges density of weak and strong acids was calculated via following equations:

$$\text{Strong acid (mmol/kg)} = \frac{M \times (V1 - V0)}{m}, \quad (1)$$

and

$$\text{Weak acid mmol/kg} = \frac{M \times (V2 - V1)}{m}, \quad (2)$$

where, *M* is the concentration of the NaOH solution (mmol/L); *m* is the dry weight of the CNCs samples (kg); *V0* is the theoretical NaOH volume used for neutralization of the added free acid (L); *V1* is the volume of NaOH solution consumed at the first intersection point (L); *V2* is the volume of NaOH solution consumed at the second intersection point (L).

2.2.3. CNCs Morphology Assessment

The apparent dynamic diameter of water dispersed CNCs 0.5 wt% at pH 6 was measured by using the dynamic light scattering (DLS) technology (mod. Litesizer 500, Anton Paar, Graz, Austria). Measures read at a 90° detection angle by DLS (90° and 25.0 ± 0.1 °C, by means of a 35 mW diode laser (λ = 658 nm) were replicated 5 times. The actual dimensions of the CNCs were confirmed via Transmission Electron Microscopy (data not shown).

2.2.4. FTIR and Raman Analysis

The FTIR spectroscopy was performed with a Perkin Elmer instrument (mod. Spectrum 100, Perkin Elmer, Milano, Italy), equipped with an ATR accessory, at room temperature. The analysis was performed on oven-dried cellulose initially brought to pH 6 and on CNCs-coated polymers (P-CNC) as well. The data were collected over 64 scans with resolutions of 4 cm^{-1} . The three types of cellulose nanocrystals were analyzed (CNC_{COOH} , CNC_{COOR} and $\text{CNC}_{\text{SO}_3\text{H}}$).

For Raman analysis, compact Raman analyzer (Cora 5X00, Anton Paar, Graz, Austria) was used with a pixel count of 1265, a laser power of 450 mW and a laser wavelength set at 785 nm with time of integration of 25,000 ms. In addition, measurements were performed on CNCs suspensions at 0.5 wt% and pH 6. These conditions were found to be effective in carrying out reproducible and complementary tests. A method proposed by Agarwal and co-workers [31] was used to assess the change of crystallinity degree of the CNCs after the esterification. The actual degree of crystallinity (X_{Ram}) of cellulose nanocrystals was then calculated through the following Equation (3):

$$X_{787\text{-Ram}} = \frac{X_{380} - \text{Ram} + 2,0212}{0,822}, \quad (3)$$

where

$$X_{380\text{-Ram}} = \frac{\left(\frac{I_{380}}{I_{1095}}\right) - 0,0286}{0,0065}, \quad (4)$$

I_{380} and I_{1095} are bands intensities at Raman shift 380 and 1095 cm^{-1} , respectively.

2.2.5. Wide Angle X-ray Scattering (WAXS)

Wide Angle X-ray Scattering (WAXS) experiments were performed using a Rigaku DMAX-II diffractometer (Japan). Diffraction patterns were obtained in the range $10^\circ < 2\theta < 40^\circ$ with $\text{Cu K}\alpha$ radiation ($\lambda = 1.5405\text{ \AA}$) under the following conditions: 40 kV, 40 mA, step width 0.02° , time per step 2 s, divergence slit 0.25° , Soller slit 0.04 rad and antiscatter slit 0.5° . X-ray patterns are normalized on the main peak.

2.2.6. Thermogravimetric Analysis (TGA)

TGA tests were conducted (TGA 4000 Perkin Elmer, Milano, Italy) in nitrogen atmosphere on samples weighing from 5 mg to 10 mg each, with a program that provides a single heating cycle from $30\text{ }^\circ\text{C}$ to $700\text{ }^\circ\text{C}$ at $20\text{ }^\circ\text{C}/\text{min}$.

2.2.7. CNCs Coatings of Plastic Films (P-CNC)

All plastic films were previously treated by corona treatment, to increase their surface energy and promote their blending with CNCs. The activated films were then coated with the three types water dispersed CNCs at 6 wt% through a green bar coater (K control Coater model 202, Royston, SG8 0QZ UK). Coated polymers were kept in dried conditions for 48 h, and the thickness of the coating applied onto the film was assessed by a gravimetric method. Four samples ($10 \times 10\text{ cm}^2$) were weighed (m_1 , g), then the coating was removed by spraying hot water ($\sim 70\text{ }^\circ\text{C}$), and the resulting uncoated film was dried and weighed (m_2 , g).

The coating thickness (L , cm) was estimated by Equation (5), where ρ is the CNCs density assumed as 1.59 g ml^{-1} :

$$L = (m_1 - m_2)/(\rho \times 100) \quad (5)$$

From the calculation, the thickness of CNCs coating resulted to be about $1\text{ }\mu\text{m}$.

2.2.8. Optical Properties of Coated Film

The transparency of the CNCs coated films was measured at 550 nm, according to the ASTM D 1746-70, by means of a UV-VIS spectro-photometer (mod. L650, Perkin-Elmer, Milano, Italy). The haze (%) of the coated polymers was measured according to ASTM D 1003-61, with the same instrument equipped with a 150 mm integrating sphere. Each sample was replicated three times, analyzing at least four spots on each replicate.

2.2.9. Z Potential of Uncoated and CNCs-Coated PET Films

The potential Z of uncoated PET film and coated with the 3 types of CNCs was measured by streaming potential method (Surpass TM 3, Anton Paar, Graz, Australia). Streaming potential and current are measured while 0.01M KCl solution flows through a chamber of a parallelepiped shape. A double-sided tape adhesive was previously cut around the holder to make sure the tape was exactly as large as the holder. The pH was changed during the measurement with the solution of 0.05 M NaOH and 0.05 M HCl. Prior to performing the measurements, the calibration of pH-meter and conductivity meter was required. It was also necessary to remove air bubbles and rinse the samples with the solution to collect reliable data. For each pH, the Z potential was measured 4 times for 3 replications.

2.2.10. Water Contact Angles Assessment

Dynamic contact angles of the plastic film coated with the 3 types of cellulose nanocrystals were determined. The sessile drop method was used by gently dropping a droplet of $4.0 \pm 0.5 \mu\text{L}$ of distilled water onto the coated film. Measurements were run at room temperature (40%RH) on five different positions for each sample for about 200 s. The instrument used was an OCA 15 Plus angle goniometer (Data Physics Instruments GmbH, Filderstadt, Germany), equipped with a high-resolution CCD camera, a high-performance digitizing adapter (Data Physics Instruments GmbH, Filderstadt, Germany) and SCA20 software (Data Physics Instruments GmbH, Filderstadt, Germany) for contact angle measurements.

2.2.11. Corona-Treatment of CNCs-Coated Films and Lamination

Prior to proceeding with the lamination process with the solvent-based polyurethanic adhesive, coated plastic films with the three types of cellulose nanocrystals were subjected to corona-discharge to yield the functionalization of cellulose nanocrystals surface thereby improving the grafting of adhesives during the lamination.

Two-component polyurethane solvent based adhesive system [mixing ratio 100:10:83 (OH: NCO: Solvent)] and 13 s viscosity 25°C was used to laminate the coated plastic films via a manual cold roll laminator and finally left for 7-day maturation at 40°C for curing and cross-linkage.

2.2.12. Gas Permeability Measurement and Peeling Test

All the oxygen permeability measurements of coated and laminated films were performed by an isostatic permeabilimeter (mod. Multiperm, PERMTECH S.r.l., PieveFosciana, Italy), according to ASTM standard methods (D-3985 and F-1249 respectively). The oxygen permeability (PO_2 , $\text{cm}^3 \text{m}^{-2} \text{d}^{-1} \text{bar}^{-1}$) of CNCs coated and laminated films were measured at 25°C under 50% and 80% RH on the coated side of the film.

For the peeling test of laminated films, measurements were carried out on specimens cut according to ATM-D882-09 and, subsequently, the values of stiffness, breaking strength and elastic modulus were collected.

3. Results and Discussion

3.1. Characterization of CNCs Properties

3.1.1. Light Scattering Characterization

CNC_{SO₃H} showed smaller hydrodynamic diameter and Z potential than those of CNC_{COOH} and CNC_{COOR}, however, the three types of CNCs dispersions showed similar values of polydispersity index, proving that crystals dimensions were well distributed in the water media (Table 1).

Table 1. Properties of dispersed cellulose nanocrystals.

CNCs Properties	CNC _{SO₃H}	CNC _{COOH}	CNC _{COOR}
Hydrodynamic diameter (nm)	130.55 ± 2.35	176.78 ± 3.52	175.02 ± 0.53
Z potential at pH (mV)	−29.60 ± 0.71	−35.65 ± 0.21	−36.30 ± 0.42
Conductivity (mS cm ^{−1})	1.31 ± 0.05	0.82 ± 0.04	1.37 ± 0.07
Polydispersityindex (%)	27.53 ± 0.51	25.24 ± 0.48	25.3 ± 0.53

3.1.2. FTIR and Raman Spectra of Dried Cellulose Nanocrystals

Figure 1a reports the FTIR spectra of the three CNCs samples. Spectrum relative to CNC_{COOR} sample showed a peak at 1743.76 cm^{−1} that can be attributed to the carbonyl stretching in esters. The presence of this peak is a strong proof of the successful functionalization of the cellulose nanocrystals during the process of chemical modification. All three hydroxyl groups of the cellobiose unit are reactive and can participate to the esterification reaction; moreover, it is worth reporting that in situ esterification used in this work can occur on CNCs surface or inside crystals [23,32].

After studying the kinetic reaction rate of oxidation and hydrolysis of cellulosic raw materials (hybrid poplar) during CNCs production by APS, Jiang et al. (2017) reported that, compared to hydrolysis, the oxidation takes much longer (>10 h) to occur [33]. Therefore, in this work, where raw cotton linters and CNC_{SO₃H} were put together, it was assumed that the CNCs esterification occurred within 10 h (i.e., a color shift considered to be an indicator of esterification occurred after 2 h) following three steps in this order: (1) rapid oxidation of more reactive −OH groups of already-present crystals CNC_{SO₃H} to introduce carboxylates groups on their surface forming CNC_{COOH}; (2) cotton linters hydrolysis which makes reactive −OH groups more available for the esterification; (3) competition between esterification and oxidation. Esterification takes place between CNC_{COOH} (1) and a part of reactive −OH groups (2), while the residues of reactive −OH are oxidized to form −COOH, which may not participate in the esterification, as they cannot find free reactive −OH groups. We are testing the same process using CNCs prepared in different ways and, combined with other raw materials, controlling the time of the esterification. In the future, it would also be very important to investigate the ideal proportions between the raw materials and the CNCs, and to evaluate the degree of substitution during the esterification. Although the esterification involves hydroxyl groups (−OH), the signal at around 3350 cm^{−1} does not change significantly, because it can be hypothesized that many −OH groups do not contribute to the esterification.

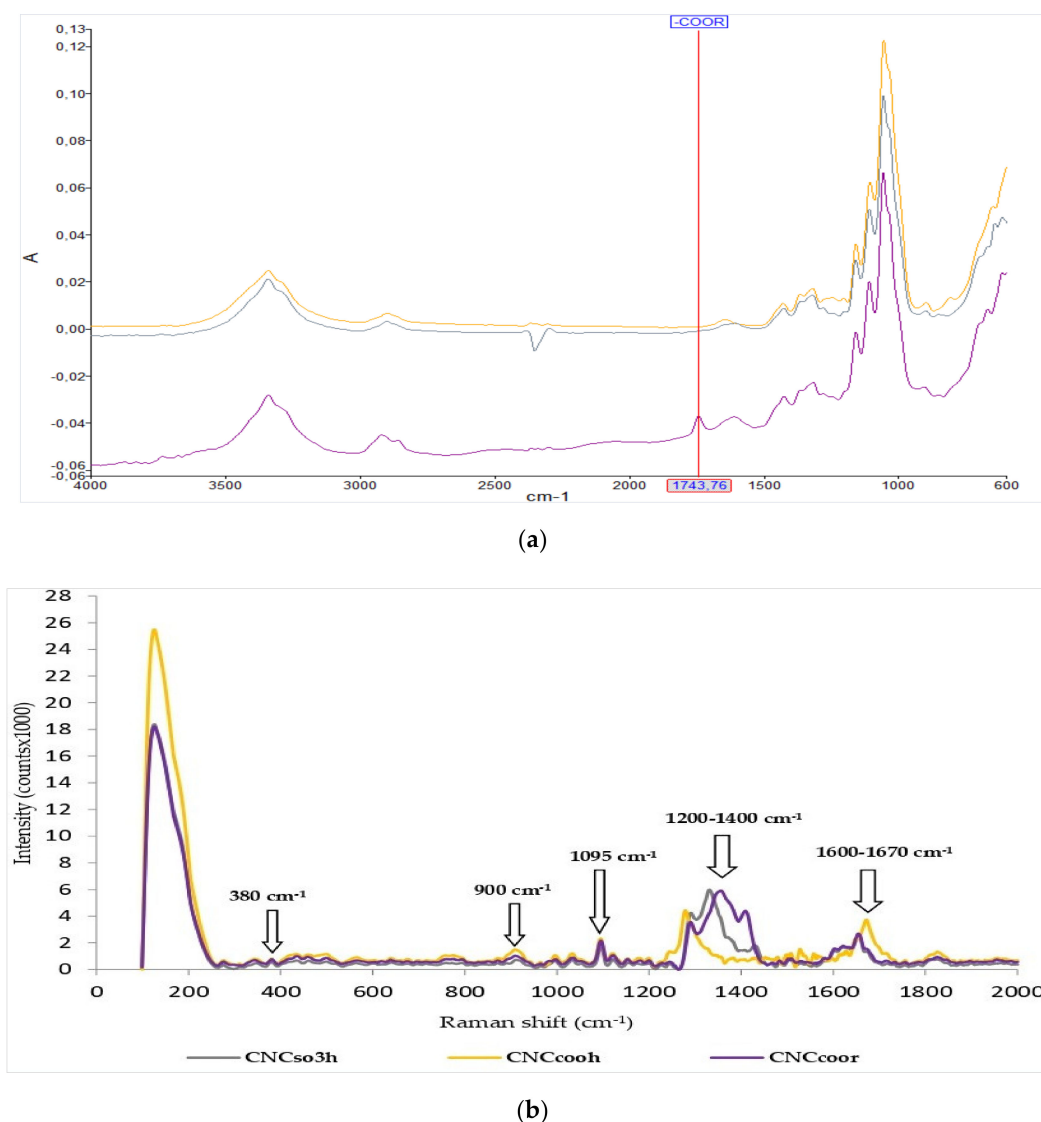


Figure 1. (a) Fourier-transform infrared spectroscopy (FTIR) spectra of the three types of cellulose nanocrystals (CNCs): CNC_{SO₃H} (yellow), CNC_{COOR} (violet) and CNC_{COOH} (green). (b) Raman analysis of the three CNCs productions: CNC_{SO₃H} (yellow), CNC_{COOH} (green) and CNC_{COOR} (violet).

From the Raman spectra (Figure 1b), the band at 900 cm⁻¹ in the spectra of cellulose is known to be associated with increased disorder [31], and therefore it was hypothesized that CNC_{COOH} were less ordered, due to their negative charges. Moreover, the regions (1200–1400 cm⁻¹) are attributed to –CH₃ bending and –COH in-plane bending motions. The bands in that region were sharper and less intense in CNC_{SO₃H}, with respect to CNC_{COOH} and CNC_{COOR}. More importantly, calculated X785-Ram values, which represent the degree of crystallinity, were 63.7%; 62.64% and 60.14% for CNC_{COOR}, CNC_{COOH} and CNC_{SO₃H}, respectively. Such similar values showed that the esterification did not affect the degree of crystallinity of the CNCs significantly. Even though Raman spectra showed differences between the three types of crystals, carbonyl groups (carboxyl and ester) were not detected, and that might be attributed to the interference of the water. Future investigations have to be carried out in order to find out the impact of the concentration of the colloidal suspension of CNCs on the measurements.

3.1.3. Z Potential Versus pH of Dispersed Cellulose Nanocrystals

Based on the values of their Z potential, the three types of CNCs suspensions showed colloidal stability at pH values ranged between 4 and 10, because negative charges ($-\text{COO}^-$ and $-\text{OSO}_3^-$) lead to a strong electrostatic repulsion in a kinetic system.

As Figure 2 reveals, the independence of the Z potential values versus pH of the CNC_{COOR} were rather constant, and higher at alkaline pH due to presence of both types of negative charges on their surface (residual carboxylates and sulfate half ester). In contrast, Z potential values of $\text{CNC}_{\text{SO}_3\text{H}}$ were the lowest and the most constant ones, while those of CNC_{COOH} fluctuated with pH change. Such behavior was expected since the CNC_{COOH} charges deprotonate to $\text{CNC}_{\text{COO}^-}$, while ester and sulfate half esters groups are more stable with pH change. Furthermore, at more acidic pH (5–6), Z potential values were found higher than those of the alkaline pH: according to a recent work, this behavior is attributed to the carboxylate ions present in colloidal suspensions [34]. It is worth noting that hydroxyl groups alone are not responsible for negative surface charges, since they are typically protonated under $\text{pK}_a > 12$. Such fact-based observation was strongly confirmed in CNCs suspension obtained by HCl, which exhibits a lack of colloidal stability because of the absence of negative charges [35].

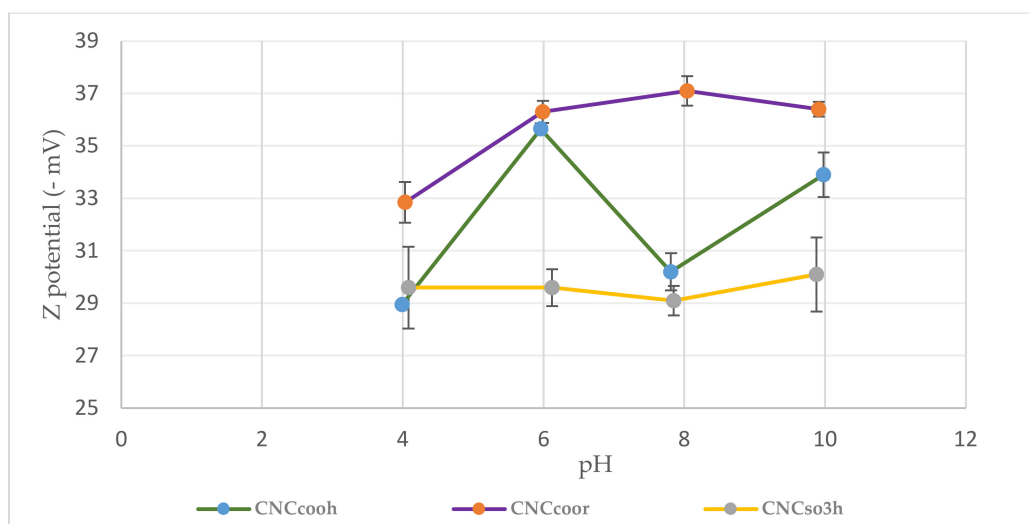


Figure 2. Z potential values versus pH of CNCs with carboxylic (CNC_{COOH}), sulfate half ester ($\text{CNC}_{\text{SO}_3\text{H}}$) and ester groups (CNC_{COOR}).

As a result of that, the pH of the CNC_{COOH} and CNC_{COOR} dispersion must be appropriately adjusted before the coating process to guarantee a higher colloidal stability and a subsequent more uniform and stronger adhesion with plastic films.

3.1.4. Charges Density by Conductometric Titration

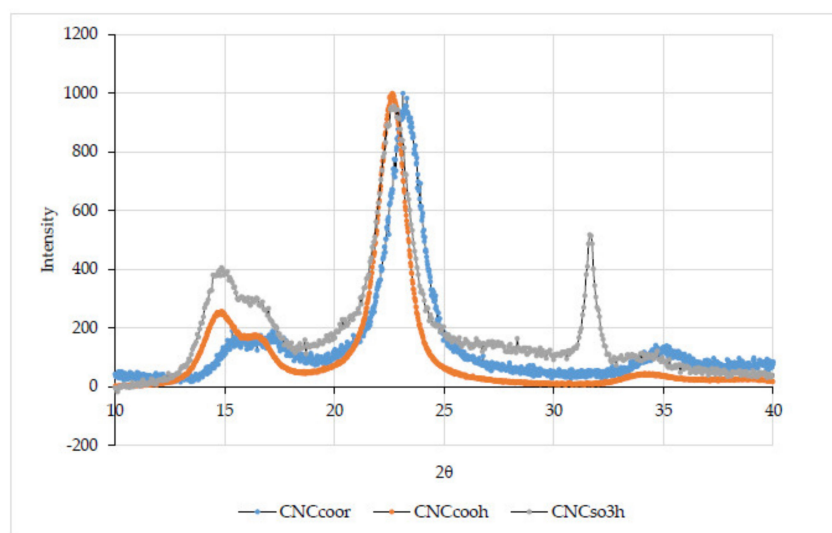
From the conductometric titration (Table 2), the concentration of weak acid ($-\text{COOH}$) derived was 0.52 mmol/kg for CNC_{COOH} , while the concentration of strong acid ($-\text{OSO}_3\text{H}$) was 0.3 mmol/kg for $\text{CNC}_{\text{SO}_3\text{H}}$. As for CNC_{COOR} , the concentrations of weak and strong acids ($-\text{COOH}$ and $-\text{OSO}_3\text{H}$) were 0.63 and 0.25 mmol/kg, respectively. It can be confirmed that CNC_{COOR} have the highest charges density attributed to total charges, which was the result of residuals of carboxylic groups and sulfate half ester groups which remained after the esterification.

Table 2. Total charges density of the three types of cellulose nanocrystals, mean \pm standard deviation ($n = 3$).

Types of Cellulose Nanocrystals	Total Charges Density (mmol/kg)
CNC _{SO₃H}	0.30 \pm 0.04
CNC _{COOH}	0.52 \pm 0.07
CNC _{COOR}	0.88 \pm 0.06

3.1.5. Wide Angle X-ray Scattering (WAXS)

Figure 3 reports the WAXS diffractograms for CNC_{COOH}, CNC_{COOR} and CNC_{SO₃H}. All three samples showed similar diffraction patterns. In particular, the CNC_{SO₃H} diffractogram is characterized by three main peaks at $2\theta = 14.79^\circ$, 16.58° and 22.83° , respectively. These peaks were very similar to the ones detected for oxidized CNC_{COOH} sample at $2\theta = 15.05^\circ$, 16.61° and 22.75° . As already reported [13], both CNC_{COOH} and CNC_{SO₃H} patterns are consistent with the I β phase crystalline pattern of cellulose. A spurious peak was also detected at $2\theta = 32^\circ$ for CNC_{SO₃H} and was attributed to a residue of Na₂SO₄, likely coming from the synthesis. CNC_{COOR} showed a similar crystalline pattern with respect to the other two CNCs samples. Peaks were shifted at $2\theta = 15.98^\circ$; 17.55° ; 23.26° , and an additional peak was detected at $2\theta = 35.26^\circ$.

**Figure 3.** Wide Angle X-ray Scattering (WAXS) diffractograms for all three samples.

In addition, the peaks appeared less sharp when compared to the other two analyzed samples. Such behavior can be explained by taking into account a more significant presence of amorphous phase, which partially hinders the detection of the crystalline phase.

The preservation of the crystalline pattern demonstrated that the esterification reaction did not affect the crystalline structure of CNCs. Crystallinity of CNCs used for coating is mandatory when aiming at reliable barrier features.

In particular, according to previous reports [36,37] cellulose is characterized by a peak around $2\theta = 22^\circ$ – 23° which is attributable to the (200) crystallographic plane of cellulose I. The amorphous phase is usually detectable at $2\theta = 18^\circ$. Therefore, the analysis of the diffractograms allowed to calculate the data using the Segal Method [38]. CNC_{COOR}, CNC_{COOH} and CNC_{SO₃H} showed a crystallinity index of 81%, 83% and 87%, respectively. The data are in good agreement with previous observations: CNC_{COOR} show the lowest crystallinity among the tested samples, but, as shown by Raman data, all three types of CNCs appear to have very similar degrees of crystallinity.

3.1.6. Thermogravimetric Analysis (TGA)

TGA analyses were performed in order to compare the thermal stability of the three samples. TGA data are reported in Figure 4, showing significantly different behaviors for the three samples.

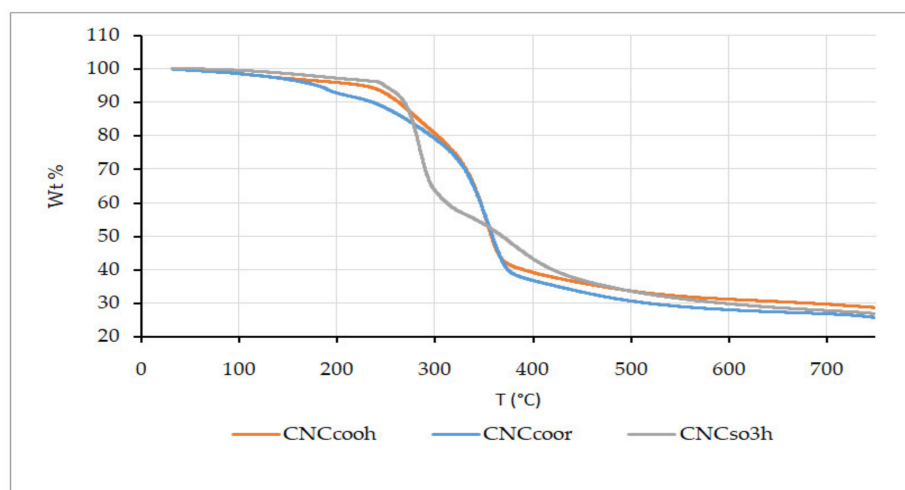


Figure 4. Thermal degradation pathways for the three samples.

It appeared that $\text{CNC}_{\text{SO}_3\text{H}}$ sample started later its degradation, when compared to CNC_{COOH} and CNC_{COOR} . These different degradation trends can be explained by the different behaviors of the superficial functional groups and their different thermal resistance. In particular, $-\text{SO}_3\text{H}$ groups are more thermally stable than $-\text{COOH}$ and $-\text{COOR}$ groups. More specifically, acidic moieties can also promote an increase of the degradation of the CNCs, through acidic catalysis. In addition, they can easily decarboxylate, contributing to the weight loss. Similarly, $-\text{COOR}$ moieties can not only lose CO_2 as preferred degradation pathway, but can also liberate $-\text{COOH}$ groups, having detrimental effects on the thermal stability of the whole system. That being said, CNC_{COOH} and CNC_{COOR} showed similar degradation pathways, yielding superimposable graphs between 300 °C and 400 °C. In addition, the beginning of the degradation started at lower temperatures for CNC_{COOR} and was likely promoted by the amorphous regions detected through WAXS analyses. $\text{CNC}_{\text{SO}_3\text{H}}$ started later their degradation, but the weight loss increased faster with respect to the other two samples, as the loss of $-\text{SO}_3\text{H}$ groups started at around 250 °C.

All three samples did not degrade completely in the testing conditions, resulting in similar quantities of carbonaceous residues.

3.2. Characterization of CNCs-Coated Plastics

3.2.1. Z Potential of CNCs Coated and Uncoated PET Film Versus pH

Z potential and contact angle were employed to assess the hydrophobicity of uncoated and CNCs-coated PET films. From the data reported in Figure 5, PET films coated with the three types of cellulose nanocrystals showed similar behavior, Z potential increases with the increase in pH values. Uncoated PET film has its isoelectric point at pH 4 while PET films coated with $\text{CNC}_{\text{SO}_3\text{H}}$, CNC_{COOH} and CNC_{COOR} have their isoelectric point at pH 1.6, 2.08 and 2.7, respectively. According to analytical instrumentation and data interpretation (SurpassTM 3), the isoelectric point found at a pH close to 4, and lower Z potential values found at $\text{pH} \approx 6$, indicate that the material exhibits less charges density. Based on the above, uncoated PET film appeared to be the material, which exhibits the lowest charges density followed by PET- CNC_{COOR} , PET- $\text{CNC}_{\text{SO}_3\text{H}}$ and PET- CNC_{COOH} .

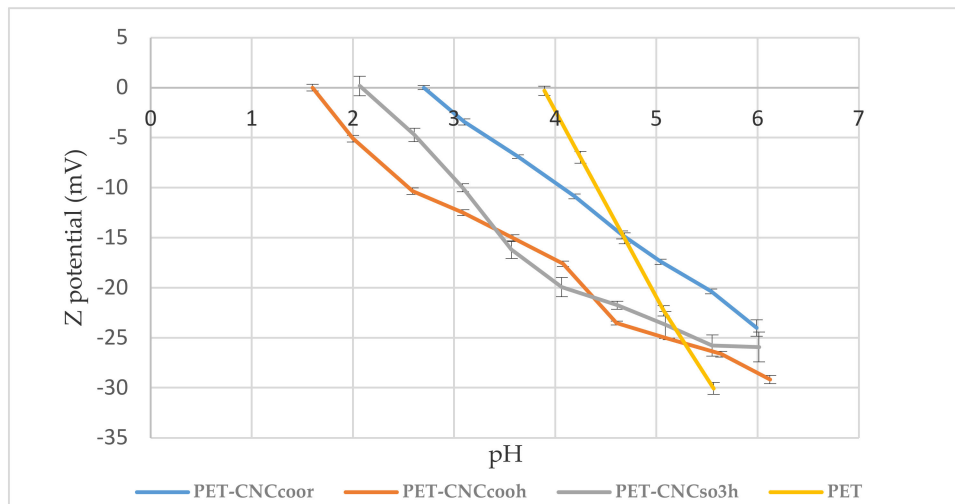


Figure 5. Z potential values versus pH of uncoated and coated PET film with the three types of cellulose CNCs ($n = 3$).

In contrast, the hydrodynamic water contact showed a different behavior (Figure 6). There was an immediate decay in water contact angle of PET films coated with esterified CNCs. It was observed that the drop of water was not absorbed by the CNC_{COOR} coated PET film, but it just expanded rapidly on the surface. PET films coated with $\text{CNC}_{\text{SO}_3\text{H}}$ and CNC_{COOH} have similar trends and decay rate over measurement time.

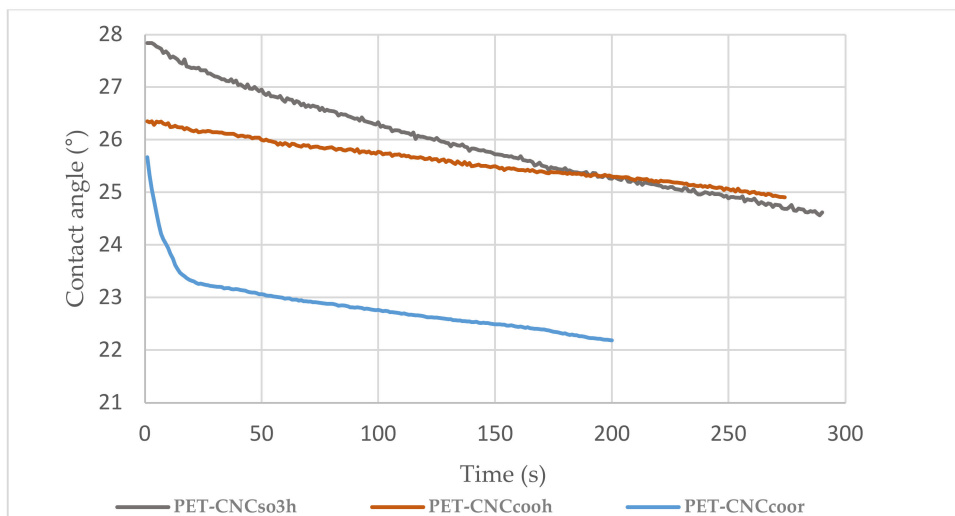


Figure 6. Water contact angle values versus time of PET film coated with the three types of cellulose nanocrystals.

3.2.2. FTIR of Corona-Treated and Untreated CNCs-Coated PET Film

The corona treatment was aimed at offsetting the lack of affinity and reinforcing the adhesion between CNCs and adhesive. As outlined in Figure 7a–c, the peaks formed during the corona-treatment can be observed. The ozone treatment usually oxidizes functionally chemical groups of the cellulose nanocrystals surface. However, that oxidation was less pronounced in the already-oxidized cellulose nanocrystals (CNC_{COOH}), while it was much more marked on esterified CNCs (CNC_{COOR}) and $\text{CNC}_{\text{SO}_3\text{H}}$ surface (Figure 7a–c), with the formation of carbonyl groups (carboxyl and ester) between 1645 cm^{-1} and 1750 cm^{-1} . These polar groups would contribute to improve the adhesion between CNCs coatings and the polyurethanic adhesive.

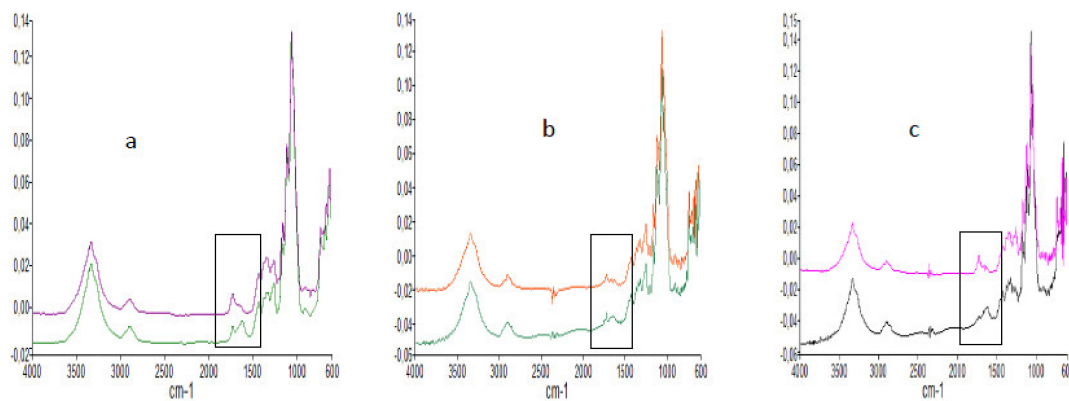


Figure 7. (a) PET-CNC_{COOR} (green) and corona treated PET-CNC_{COOR} (violet); (b) PET-CNC_{SO₃H} (green) and corona treated PET-CNC_{SO₃H} (red); and (c) PET-CNC_{COOH} (black) and corona treated PET-CNC_{COOH} (violet).

3.2.3. Oxygen Permeability of Coated Polymers (P-CNC)

When comparing the oxygen permeability of coated polymers with the three types of cellulose nanocrystals, the difference is evident at both RH (50% and 80%). The improvements of the oxygen barrier properties are much higher on polymers coated CNC_{COOR}, following by those coated with CNC_{COOH} and CNC_{SO₃H} (Figure 8). This demonstrates the relevance of the esterification of cellulose nanocrystals, which allowed creating structures less sensitive to water, without modifying the crystallinity or compromising the integrity of the crystals. Although the oxygen barrier was enhanced in the three cases, the oxygen permeability of the coated polymers showed a significant loss of barrier properties at high relative humidity (80%), due to a strong affinity between the CNCs coatings and water.

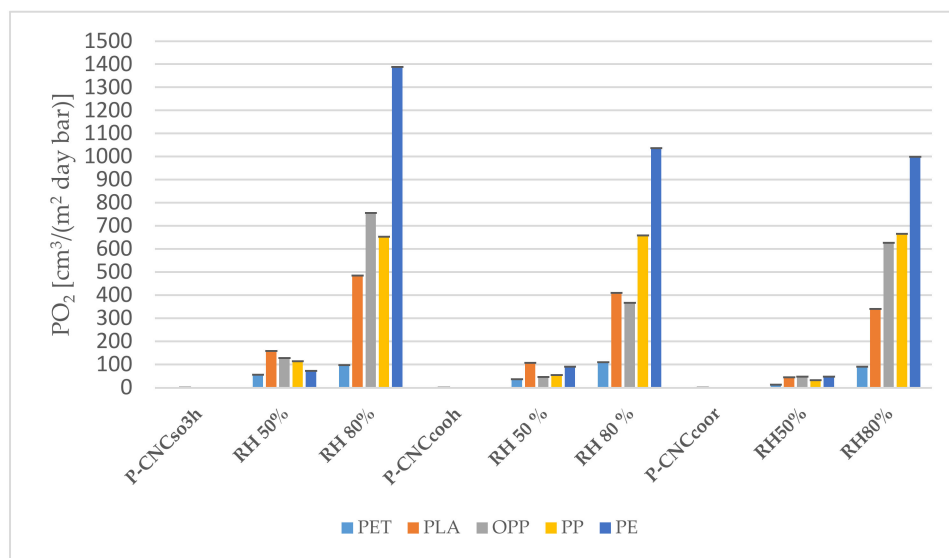
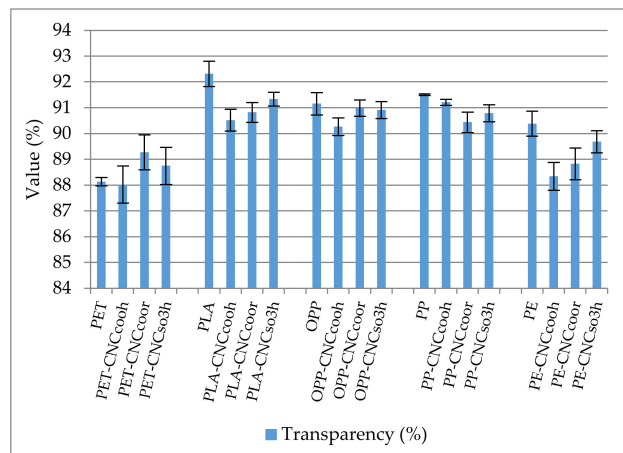


Figure 8. Oxygen permeability of polymers coated with CNC_{SO₃H}, CNC_{COOH} and CNC_{COOR} at 50% and 80% RH.

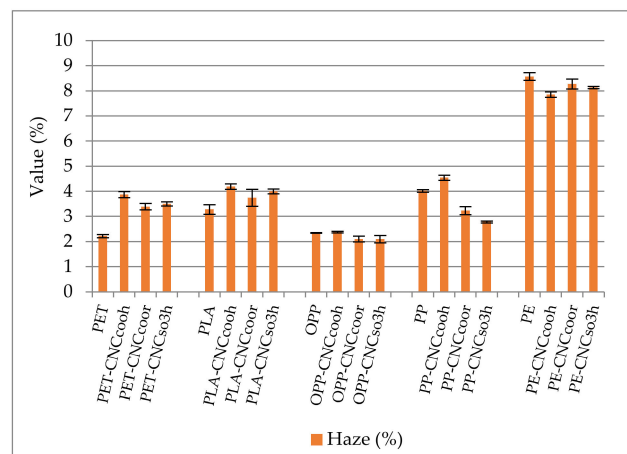
3.2.4. Haze and Transparency of Coated and Uncoated Polymers

Uncoated and CNCs-coated polymers (P-CNC) showed similar values of haze and transparency, proving that the coating of polymers with the three types of polymers has not significantly affected the optical properties the original plastic films (Figure 9a,b). However, the haze values of coated and uncoated PLA and PE films were slightly different, and this was attributed to their chemical-physical

modification, which occurs during the corona treatment. More importantly, the esterification did not modify the optical properties of the cellulose nanocrystals.



(a)



(b)

Figure 9. (a) Transparency (blu) and (b) haze (orange) of uncoated and coated polymers with the three types of CNCs calculated from the mean \pm standard deviation ($n = 4$).

3.3. Characterization of Laminated CNCs-Coated PET Films (P-CNC-P)

3.3.1. Delamination Test

In light of the data from a peeling test of laminated plastic films (Table 3) collected according to ASTM-D882-09, stiffness, breaking strength and elastic modulus were all acceptable. Different values of the delamination test proved that the strength of the adhesion strongly depends on the surface chemistry of the polymers and cellulose nanocrystals. Furthermore, it can be indicated that the laminated plastic films based on esterified cellulose nanocrystals displayed the best performance in terms of mechanical properties. These values of a peeling test can be further improved if the lamination is set on an industrial scale. Finally, it can be confirmed that the corona-treatment subjected to coated polymers prior the lamination definitely led to a reinforcement of the adhesion between the cellulose nanocrystals and the adhesive.

Table 3. Results of peeling test of laminated coated-polymers.

Laminated Polymers	P-CNC _{SO₃H} -P	P-CNC _{COOH} -P	P-CNC _{COOR} -P
Elastic Modulus (N/m)	13,000–36,000	14,000–43,000	18,000–28,000
Breaking Strength (N/m)	14–20	16–60	22–74
Stiffness (N/m)	650–7000	3600–5000	3500–8300

3.3.2. Oxygen Permeability of Laminates with CNCs Coated Films (P-CNC-P)

Table 4 illustrates the values of oxygen permeability expressed in $\text{cm}^3/(\text{m}^2 \times 24 \text{ h} \times \text{bar})$ of laminated coated-films measured at 50% and 80% RH at 23 °C. The lamination of coated films further improved the gas barrier for all the three types of cellulose nanocrystals.

Table 4. Oxygen permeability of laminated coated-polymers at RH 50–80%, calculated from the mean \pm standard deviation ($n = 3$).

P-CNC _{SO₃H} -P	50% RH	80% RH
OPP- CNC _{SO₃H} /PE	<0.06	1.2 \pm 0.25
OPP- CNC _{SO₃H} /PLA	40 \pm 0.15	320 \pm 3.5
PET- CNC _{SO₃H} /PE	0.25 \pm 0.15	1.107 \pm 0.25
PET- CNC _{SO₃H} /PP	<0.06	<0.06
P-CNC _{COOH} -P	50% RH	80% RH
OPP- CNC _{COOH} /PE	<0.06	<0.06
OPP- CNC _{COOH} /PLA	12.41 \pm 3.5	201.11 \pm 3.5
PET- CNC _{COOH} /PE	<0.06	<0.06
PET- CNC _{COOH} /PP	<0.06	<0.06
P-CNC _{COOR} -P	50% RH	80% RH
OPP- CNC _{COOR} /PE	<0.06	<0.06
OPP- CNC _{COOR} /PLA	3.78 \pm 3.5	103.55 \pm 3.5
PET- CNC _{COOR} /PE	<0.06	<0.06
PET- CNC _{COOR} /PP	<0.06	<0.06

The lamination technique was very effective in blocking water from the surrounding environment to disrupt or modify the crystallinity network of the cellulose nanocrystal's coatings. In addition, gas barrier properties were not lost after the lamination, and that proved the excellent chemical affinity between the adhesive and the CNCs. The combination of both techniques, i.e., chemical modification and lamination, to mitigate the swelling of the coatings of cellulose nanocrystals surface resulted the most effective approach to strongly enhance the gas barrier properties even at higher relative humidity. It bears observing that sealable and hydro-repellent plastics, such as PP and PE, showed better O₂ under 50% and 80% RH, compared to PLA, which is a water sensitive polymer. To this regard, however, CNC_{COOR} proved their effectiveness in reducing the PLA oxygen permeability. In particular, they reduced the permeability by a ten-fold factor with respect to CNC_{SO₃H} at 50% RH, but positive effects were also recorded with respect to CNC_{COOH} even at 80% RH.

4. Conclusions

Three different cellulose nanocrystals derived species were compared in their properties, aiming for a possible application in the food packaging sector. All the samples were fully characterized and employed as coatings on different types of plastic films. The main problem to be sorted out was the sensibility of the cellulose nanocrystals to moisture that hampered their incorporation into food

packaging. It was noted that barrier gas properties of cellulose nanocrystals were effective in the absence of humidity, but were compromised in a humid environment. Through this work, it has been shown that the esterification of cellulose nanocrystals has significantly improved the gas barrier, compared to the unmodified ones. In addition, the oxygen permeability of laminated coated-polymers showed very low values, even in high relative humidity (80% RH), which is the confirmation that the lamination has definitely isolated the CNCs coatings from the moisture and that subsequently, it could favor such materials to be used for food shelf-life extension. From the results of the delamination test, it can be observed that the stiffness, elastic modulus and elongation at the end are relevant for all delamination tests of polymers. It is very important to indicate that the lamination of polymers coated with esterified cellulose nanocrystals were the best in terms of reducing the gas permeability, even in higher relative humidity, followed by laminated polymers coated with CNC_{COOH} and CNC_{SO₃H}. Furthermore, sealable plastics selected for the lamination would enable a swift application of CNCs in food packaging, replacing the oil-based materials, such as EVOH and PVDC, that are used today. Such high-performance multi-layer laminates based on a very thin layer of CNCs ($\approx 1 \mu\text{m}$) would imply a paradigm change for the effective development of advanced materials, taking care of environmental protection and the principles of a circular economy.

Author Contributions: G.F., S.G., M.A.O. and L.P. were all involved in the conceptualization and the methodology of the project, design and realization of experiments, design of the project and analysis of the data as well as in the writing of the paper. L.P. was also involved in the supervision and administration of the project and funding acquisition. All authors have read and agreed to the published version of the manuscript.

Funding: This research was funded by European Union's Horizon 2020 Research and innovative Program under grant agreement number: 720326.

Conflicts of Interest: The authors declare no conflict of interest.

References

1. Araki, J.; Wada, M.; Kuga, S. Steric Stabilization of a Cellulose Microcrystal Suspension by Poly(ethylene glycol) Grafting. *Langmuir* **2001**, *17*, 21–27. [[CrossRef](#)]
2. Beck-Candanedo, S.; Roman, M.; Gray, D.G. Effect of Reaction Conditions on the Properties and Behavior of Wood Cellulose Nanocrystal Suspensions. *Biomacromolecules* **2005**, *6*, 1048–1054. [[CrossRef](#)]
3. Cherhal, F.; Cousin, F.; Capron, I. Influence of Charge Density and Ionic Strength on the Aggregation Process of Cellulose Nanocrystals in Aqueous Suspension, as Revealed by Small-Angle Neutron Scattering. *Langmuir* **2015**, *31*, 5596–5602. [[CrossRef](#)] [[PubMed](#)]
4. Reid, M.S.; Villalobos, M.; Cranston, E.D. Benchmarking Cellulose Nanocrystals: From the Laboratory to Industrial Production. *Langmuir* **2016**, *33*, 1583–1598. [[CrossRef](#)] [[PubMed](#)]
5. Leung, A.C.W.; Hrapovic, S.; Lam, E.; Male, K.B.; Mahmoud, K.A.; Liu, Y.; Luong, J.H.T. Characteristics and Properties of Carboxylated Cellulose Nanocrystals Prepared from a Novel One-Step Procedure. *Small* **2010**, *7*, 302–305. [[CrossRef](#)]
6. Habibi, Y.; Chanzy, H.; Vignon, M.R. TEMPO-mediated surface oxidation of cellulose whiskers. *Cellul.* **2006**, *13*, 679–687. [[CrossRef](#)]
7. Reid, M.S.; Villalobos, M.; Cranston, E. Cellulose Nanocrystal Interactions Probed by Thin Film Swelling to Predict Dispersibility. *Nanoscale* **2016**, *8*, 12247–12257. [[CrossRef](#)]
8. Shimizu, M.; Saito, T.; Isogai, A. Bulky quaternary alkylammonium counterions enhance thenanodispersibility of 2,2,6,6-tetramethylpiperidine-1-oxyl-oxidized cellulose in diverse solvents. *Biomacromolecules* **2014**, *15*, 1904–1909. [[CrossRef](#)]
9. Cheng, N.; Wen, Y.; Wang, L.; An, X.; Zhu, X.; Ni, Y. Adsorption of polyethylene glycol (PEG) onto cellulose nano-crystals to improve its dispersity. *Carbohydr. Polym.* **2015**, *123*, 157–163. [[CrossRef](#)]
10. Fakhouri, F.M.; Casari, A.C.A.; Mariano, M.; Yamashita, F.; Innocentini-Mei, L.H.; Soldi, V.; Martelli, S.M. Effect of a gelatin-based edible coating containing cellulose nanocrystals (CNC) on the quality and nutrient retention of fresh strawberries during storage. *IOP Conf. Ser. Mater. Sci. Eng.* **2014**, *64*, 012024. [[CrossRef](#)]
11. Fotie, G.; Limbo, S.; Piergiovanni, L. Effectiveness of cellulose nanocrystals (cncs) application as bio-based oxygen barrier for shelled walnuts shelf-life extension. *Ital. J. Food Sci.* **2017**, *6*.

12. Fotie, G.; Amoroso, L.; Limbo, S.; Muratore, G.; Piergiovanni, L. Food life extension by cellulose nanocrystals coatings. *Ital. J. Food Sci.* **2019**, 8–14.
13. Rampazzo, R.; Alkan, D.; Gazzotti, S.; Ortenzi, M.A.; Piva, G.; Piergiovanni, L. Cellulose Nanocrystals from Lignocellulosic Raw Materials, for Oxygen Barrier Coatings on Food Packaging Films. *Packag. Technol. Sci.* **2017**, *30*, 645–661. [[CrossRef](#)]
14. Belbekhouche, S.; Bras, J.; Siqueira, G.; Chappey, C.; Lebrun, L.; Khelifi, B.; Marais, S.; Dufresne, A. Water sorption behavior and gas barrier properties of cellulose whiskers and microfibrils films. *Carbohydr. Polym.* **2011**, *83*, 1740–1748. [[CrossRef](#)]
15. Gicquel, E.; Martin, C.; Yanez, J.G.; Bras, J. Cellulose nanocrystals as new bio-based coating layer for improving fiber-based mechanical and barrier properties. *J. Mater. Sci.* **2016**, *52*, 3048–3061. [[CrossRef](#)]
16. Fotie, G.; Rampazzo, R.; Ortenzi, M.A.; Checchia, S.; Fessas, D.; Piergiovanni, L. The Effect of Moisture on Cellulose Nanocrystals Intended as a High Gas Barrier Coating on Flexible Packaging Materials. *Polymers* **2017**, *9*, 415. [[CrossRef](#)] [[PubMed](#)]
17. Eyley, S.; Thielemans, W. Surface modification of cellulose nanocrystals. *Nanoscale* **2014**, *6*, 7764–7779. [[CrossRef](#)] [[PubMed](#)]
18. George, J.; Sabapathi, S. Cellulose nanocrystals: Synthesis, functional properties, and applications. *Nanotechnol. Sci. Appl.* **2015**, *8*, 45–54. [[CrossRef](#)]
19. Lam, E.; Male, K.B.; Chong, J.H.; Leung, A.C.; Luong, J.H.T. Applications of functionalized and nanoparticle-modified nanocrystalline cellulose. *Trends Biotechnol.* **2012**, *30*, 283–290. [[CrossRef](#)]
20. Bendahou, A.; Hajlane, A.; Dufresne, A.; Boufi, S.; Kaddami, H. Esterification and amidation for grafting long aliphatic chains on to cellulose nanocrystals: A comparative study. *Res. Chem. Intermed.* **2014**, *41*, 4293–4310. [[CrossRef](#)]
21. Berlioz, S.; Molina-Boisseau, S.; Nishiyama, Y.; Heux, L. Gas-Phase Surface Esterification of Cellulose Microfibrils and Whiskers. *Biomacromolecules* **2009**, *10*, 2144–2151. [[CrossRef](#)] [[PubMed](#)]
22. Gazzotti, S.; Farina, H.; Lesma, G.; Rampazzo, R.; Piergiovanni, L.; Ortenzi, M.A.; Silvani, A. Polylactide/cellulose nanocrystals: The in situ polymerization approach to improved nanocomposites. *Eur. Polym. J.* **2017**, *94*, 173–184. [[CrossRef](#)]
23. Braun, B.; Dorgan, J.R. Single-Step Method for the Isolation and Surface Functionalization of Cellulosic Nanowhiskers. *Biomacromolecules* **2009**, *10*, 334–341. [[CrossRef](#)] [[PubMed](#)]
24. Çetin, N.S.; Tingaut, P.; Özmen, N.; Henry, N.; Harper, D.P.; Dadmun, M.D.; Sèbe, G. Acetylation of Cellulose Nanowhiskers with Vinyl Acetate under Moderate Conditions. *Macromol. Biosci.* **2009**, *9*, 997–1003. [[CrossRef](#)] [[PubMed](#)]
25. Habibi, Y.; Lucia, L.A.; Rojas, O.J. Cellulose Nanocrystals: Chemistry, Self-Assembly, and Applications. *Chem. Rev.* **2010**, *110*, 3479–3500. [[CrossRef](#)]
26. Arrieta, M.P.; Fortunati, E.; Dominici, F.; Rayón, E.; López-Martínez, J.; Kenny, J.M. PLA-PHB/cellulose based films: Mechanical, barrier and disintegration properties. *Polym. Degrad. Stab.* **2014**, *107*, 139–149. [[CrossRef](#)]
27. Fortunati, E.; Peltzer, M.; Armentano, I.; Torre, L.; Jiménez, A.; Kenny, J.M. Effects of modified cellulose nanocrystals on the barrier and migration properties of PLA nano-biocomposites. *Carbohydr. Polym.* **2012**, *90*, 948–956. [[CrossRef](#)]
28. Ferrer, A.; Pal, L.; Hubbe, M.A. Nanocellulose in packaging: Advances in barrier layer technologies. *Ind. Crop. Prod.* **2017**, *95*, 574–582. [[CrossRef](#)]
29. Zhang, Z.; Britt, I.J.; Tung, M.A. Permeation of oxygen and water vapor through EVOH films as influenced by relative humidity. *J. Appl. Polym. Sci.* **2001**, *82*, 1866–1872. [[CrossRef](#)]
30. Shah, G.P. Oxygen Barrier Biaxially Oriented Film. U.S. Patent 5,004,647, 2 April 1991.
31. Agarwal, U.P.; Atalla, R.H.; Isogai, A. Raman Spectroscopy in the Analysis of Cellulose Nanomaterials. *Chem. Stud. Success Field-Tested Evid. Based Guide* **2017**, *1251*, 75–90. [[CrossRef](#)]
32. Hasani, M.; Cranston, E.D.; Westman, G.; Gray, D.G. Cationic surface functionalization of cellulose nanocrystals. *Soft Matter* **2008**, *4*, 2238–2244. [[CrossRef](#)]
33. Jiang, H.; Wu, Y.; Han, B.; Zhang, Y. Effect of oxidation time on the properties of cellulose nanocrystals from hybrid poplar residues using the ammonium persulfate. *Carbohydr. Polym.* **2017**, *174*, 291–298. [[CrossRef](#)] [[PubMed](#)]
34. Park, J.Y.; Park, C.-W.; Han, S.-Y.; Kwon, G.-J.; Kim, N.H.; Lee, S.-H. Effects of pH on Nanofibrillation of TEMPO-Oxidized Paper Mulberry Bast Fibers. *Polym.* **2019**, *11*, 414. [[CrossRef](#)] [[PubMed](#)]

35. Bhattacharyya, L.; Rohrer, J.S. (Eds.) *Applications of Ion Chromatography for Pharmaceutical and Biological Products*; John Wiley & Sons, Inc.: Hoboken, NJ, USA, 2012.
36. Lamaming, J.; Hashim, R.; Leh, C.P.; Sulaiman, O. Properties of cellulose nanocrystals from oil palm trunk isolated by total chlorine free method. *Carbohydr. Polym.* **2017**, *156*, 409–416. [[CrossRef](#)]
37. Wada, M.; Okano, T.; Sugiyama, J. Allomorphs of native crystalline cellulose I evaluated by two equatorial d-spacings. *J. Wood Sci.* **2001**, *47*, 124–128. [[CrossRef](#)]
38. Segal, L.; Creely, J.; Martin, A.; Conrad, C.; Jr, A.M. An Empirical Method for Estimating the Degree of Crystallinity of Native Cellulose Using the X-Ray Diffractometer. *Text. Res. J.* **1959**, *29*, 786–794. [[CrossRef](#)]



© 2020 by the authors. Licensee MDPI, Basel, Switzerland. This article is an open access article distributed under the terms and conditions of the Creative Commons Attribution (CC BY) license (<http://creativecommons.org/licenses/by/4.0/>).